



ORIGINAL ARTICLE

Anticancer activity of Zinc-Sodium alginate-Polyethylene glycol- Brucine nanocomposite in gallbladder cancer NOZ cells via modulation of apoptosis and P13K/mTOR pathway



Xin Yao ^a, Lingdi Li ^b, Wei Lu ^a, Xin Yin ^c, LeiTao Cao ^{d,*}

^a Department of Interventional Therapy and Vascular Surgery, Tianjin Nankai Hospital, Tianjin 300100, China

^b Department of Oncology, Hangzhou Cancer Hospital, Hangzhou, Zhejiang 310002, China

^c Department of Traditional Chinese Medicine, Tianjin Hexi District Meijiang Street Community Health Service Center, Tianjin 300202, China

^d Department of Vascular Surgery, Dingzhou People's Hospital, Dingzhou, Hebei 073000, China

Received 21 November 2022; accepted 23 March 2023

Available online 29 March 2023

KEYWORDS

Cytotoxicity;
NOZ cells;
Apoptosis;
Nanomedicines;
PI3K/Akt/mTOR pathway

Abstract *Background:* Gallbladder cancer (GBC) is the sixth most predominant gastrointestinal tumor worldwide. Malignant tumors with distinctive biological characteristics, like the human GBC, are incredibly aggressive and challenging to diagnose and treat.

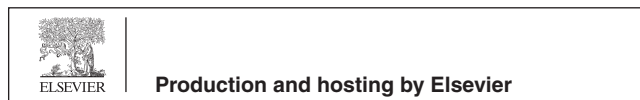
Objective: The aim of the present study is to explore the *in vitro* anticancer properties of ZAP-Brucine nanocomposites (ZAP-Bru NCs) on gallbladder cancer cells.

Methodology: The cytotoxicity of the ZAP-Bru NCs at concentrations ranging from 10 to 60 $\mu\text{g}/\text{mL}$ on the NOZ cells was assessed by an MTT study. The IC₅₀ value of ZAP-Bru NCs was found to be 5 $\mu\text{g}/\text{mL}$, which indicates that it has 50% inhibitory effects on NOZ cells than other doses. Several fluorescent staining approaches, such as dual staining and rhodamine-123 techniques, were applied to investigate the apoptosis and MMP levels in the treated NOZ cells. The generation of ROS in the treated NOZ cells was examined by DCFH-DA staining. The modifications in the expressions of inflammatory genes like NF- κB , TNF- α , IL-6, COX-2, and IL-6 in the treated NOZ cells were examined using the respective kits.

* Corresponding author.

E-mail address: caoleitao2021@sina.com (L. Cao).

Peer review under responsibility of King Saud University.



Results: ZAP-Bru NCs treatment effectively induced apoptosis in NOZ cells by increasing late and early apoptotic cell numbers. ZAP-Bru NCs also enhanced mitochondrial apoptosis through Bcl-2 protein-dependent signaling. NOZ cells phosphorylated PI3K, Akt, cyclin D1, and mTOR in response to ZAP-Bru NCs treatment. ZAP-Bru NCs treatment also inhibited the phosphorylation of Akt and mTOR in the NOZ cells. Compared to the control group, ZAP-Bru NCs-treated NOZ cells demonstrated significantly fewer proliferative cells and more apoptotic cells.

Conclusion: Accordingly, ZAP-Bru NCs could be talented medications against gallbladder cancer.

© 2023 Published by Elsevier B.V. on behalf of King Saud University. This is an open access article under the CC BY-NC-ND license (<http://creativecommons.org/licenses/by-nc-nd/4.0/>).

1. Introduction

Gallbladder cancer (GBC) is the sixth most predominant gastrointestinal tumor in the world, responsible for 80–95 percent that results in a high death rate associated with cancer (Bray et al., 2018; Strum et al., 2022). Although GBC is very infrequent in most developed nations, it affects at least 219,420 people worldwide annually. Korea, Peru, Chile, Nepal, Bangladesh, Bolivia, Japan, and the Czech Republic are among the countries with the highest death rates. In 2015, there were 10.2 deaths per 100,000 women due to GBC. It is one of Chile's most prevalent malignancies, and it is the second foremost cause of cancer-associated mortality among women (Zhu et al., 2023). The absence of characteristic signs in the initial phases and the limited availability of effective indicators lead most physicians to detect the disease at a developed and/or metastatic stage (Randi et al., 2006). To increase the clinical diagnosis of GBC, better and effective early detection techniques and treatment alternatives are required.

GBC research is difficult not only because it is a rare tumor around the world but also because human tissue samples are difficult to obtain and experimental models are lacking (Goldin et al., 2009). The use of alkylating agents and antimetabolites in current cancer treatment has a slew of side effects and is deleterious for showing toxicity (Rasmussen et al., 2010). The use of nanomaterials is one of the most cutting-edge therapy techniques (Peng et al., 2021; Huang 2021). Anticancer medications have been delivered via nanomaterials and nanostructured devices. The application of nanotechnology to medication delivery has resulted in the regulated discharge of anti-cancer therapies, which has improved their *in vivo* effectiveness (Salimpour et al., 2020; Abdollahi et al., 2021; Fernandes et al., 2015). Nanocomposites (NCs) are familiar to have characteristic anticancer effects because of their biological effects. NCs' anticancer activity is attributed to either inherent features, such as antioxidant property or apoptosis-stimulating capacity. The NCs can effectively interrelate with the tumor's surroundings, such as blood vessels or stroma, and obstruct tumor growth (Caputo et al., 2014). Metal nanocomposites are used in cancer treatment and are being developed for salutary and diagnostic approaches. It is possible to make metallic and/or metal oxide NCs for the treatment of various cancers (Mody et al., 2010).

ZAP- Brucine NPs have the potential use for cancer treatment, which has recently gained a lot of attention. However, lack of treatment with ZAP- Brucine, in particular, the underlying mechanisms of apoptosis induced by ZAP-Brucine NP therapy in cancer cells (Zhang et al., 2011). Biologically active polymers such as polyethylene glycol (PEG) produce water-soluble compounds that are especially important to the development of polymer-drug analogs (Tshweu et al., 2020). In drug delivery systems, conjugating PEG with betulinic acid (BA) enhances the solubility and specificity of drugs by increasing drug potency (Fru et al., 2021). Brucine has an outstanding anticancer influence on several types of cancer (Li et al., 2018). Colorectal cancer cells may be inhibited in their growth and migration by brucine, which

regulates the Wnt/-catenin signaling cascade (Shi et al., 2018). Hence, we hypothesized that ZAP- Brucine NPs may have effective anticancer activity against GBC. Therefore, in the current study, we synthesized the ZAP-Bru NCs and evaluated their anticancer properties in human GBC NOZ cells.

2. Material and methods

2.1. Chemicals

Polyethylene glycol, sodium alginate, and zinc oxide were acquired from Sigma Aldrich, USA. Brucine solution was procured from Loba Chemie, Germany.

2.2. The preparation of ZAP- Brucine (Zinc-Sodium alginate-Polyethylene glycol- Brucine) nanocomposites (ZAP-Bru NCs)

To synthesize ZAP-Bru NCs with an average diameter of 25 nm, 0.3 g of zinc was added to the sodium alginate solution, and then mixed to the polyethylene glycol (PEG) solution. The Zinc-Sodium alginate-PEG homogenization mixture was then encapsulated with Brucine solution. For 6 h, a continuous stirring process was performed at 80 °C with ZAP-Bru NCs. We detected the presence of a white precipitate after constant stirring and centrifuged the residue for 15 min at −4 °C. The obtained ZAP-Bru NCs were dried over three hours at 200 °C after several washes with deionized water. Further, the prepared ZAP-Bru NCs was characterized using several techniques.

2.3. Characterization of ZAP-Bru NCs

To determine absorbance spectra in the 400–1000 nm range, UV–vis spectrophotometry was performed on a Cary-50 Scan Varian instrument.

A FT-IR study was implemented to investigate the ZAP-Bru NCs for the presence of functional groups. After drying, ZAP-Bru NCs powder was used for FT-IR study and spectra were detected using Perkin-Elmer at 4000 cm^{−1} and 400 cm^{−1} range.

The PLS technique was implemented to detect the PL spectrum of ZAP-Bru NCs. Eclipse (Varian) at a width of 5 nm, 120 nm/min of scan rate, 1 nm of interval (average time 0.5 s), 600 V of voltage, and 325 nm of excitation wavelength. A time-resolved PL study was executed using a laser coupled to an optical parametric oscillator (OPO) at 10 Hz frequency at 325 nm to excite the sample. An ICCD Instaspec-V ICCD

detector and Hg lamp calibration were utilized to detect the sample emission with an Oriel f-125 monochromator graded at 400 grooves/mm.

The XL-30 Philips SEM machine equipped with EDAX was utilized to detect the morphology of the ZAP-Bru NCs. We prepared the SEM sample by dispersing the ZAP-Bru NCs in isopropyl alcohol, drop-coating them onto Al₂O₃, and drying them in the oven at 80 °C for 30 min. Finally ZAP-Bru NCs were filmed to analyze the morphology of the ZAP-Bru NCs.

On a Bruker D8 diffractometer using a copper tube, XRD patterns were acquired for the ZAP-Bru NCs. Our diffractogram analysis was conducted with the software DIFFRAC and EVA-V3.1 and the COD2013 (Crystallography Open Data, 2013) database. The Scherrer equation was used to calculate the crystal size. Using the DLS study and a Malvern ZEN3600 Zetasizer, the size of the ZAP-Bru-NCs was recognized based on Brownian motion. The sample was vortexed, ultrasonicated (at 25 kHz) for 15 min, and agitated for 2 min using an Ultrasonic probe (model disruptor), which dissolved 1 mg of ZAP-Bru NCs particles.

2.4. Collection of NOZ cells

Human GBC cell line (NOZ) was purchased from ATCC, USA, and grown on 10% FBS-enriched Dulbecco's modified eagle's medium (DMEM) with 1 % antimycotic cocktail. The cells were maintained at 37 °C in a chamber with 5% of CO₂ for 24 h. The additional tests were done with sub-cultured cells after reaching 80% confluency.

2.5. MTT assay

Before being seeded and incubated with 5 % CO₂ for 24 h, NOZ cells were plated onto 96-wellplate. After maintenance for 24 hrs, cells were treated with diverse concentrations of ZAP-Bru NCs (1, 2.5, 5, 7.5, 10 & 15 µg/ml) for 24 hrs. Then the medium was removed after the cells underwent an MTT experiment (Mossman, 1963). A microplate reader was used to detect the solution's optical density at 595 nm and determine the proportion of live cells.

2.6. ROS staining

The NOZ cells growing on 24-well plates subjected to DCFH-DA staining to detect the intracellular ROS level. After 24 h, ZAP-Bru NCs were incubated at 5 and 7.5 µg/ml concentrations at 37 °C with 5 % CO₂. 30 min were needed for staining after incubation with the DCFH-DA dye. Finally, cells were inspected under an microscope (Olympus) to find the fluorescent emitters.

2.7. Rhodamine-123 staining

Rh-123 staining was utilized to examine the permeability of the mitochondrial membrane in NOZ cells treated with ZAP-Bru NCs. The addition of 5 and 7.5 µg/ml of ZAP-Bru NCs to 24-well plates containing NOZ cells was done 24 h prior to incubation. Then cells were incubated for 30 min with 1 mMol Rhodamine 123 to stain the cells. After incubating the dyed

cells in the dark for 15 min, they were examined under a fluorescent microscope.

2.8. Dual staining

ZAP-Bru NCs treated NOZ cells were studied by dual staining to assess the apoptosis. Cells were incubated at 37 °C with 5 and 7.5 µg/ml of ZAP-Bru NCs for 24 h. The cells were stained with AO/EB after being washed with phosphate buffer (PBS) (1:1). The stained cells were viewed under a fluorescence microscope after 30 min of dark incubation.

2.9. Cellular adhesion assay

Cell adhesion assays were used to evaluate the characteristics of ZAP-Bru NCs treated NOZ cells. DMEM medium containing no serum was added to coated plates, and cells were sustained for two hrs. After 2 h, the cells were cleansed thrice with PBS and then fixed for 10 min in methanol after removing unattached cells. A microscope was used to observe and evaluate the cells after they were stained with methylene blue dye for 15 min.

2.10. Real-time PCR analysis

The RT-PCR technique was used to measured the expression levels of NF-κβ, COX2, IL-6, TNF-α, Akt, mTOR, PI3K, CyclinD1, Bcl-2, Caspase-3, and Bax in the NOZ cells. The manufacturer's protocol was followed to isolate total RNA from tissue samples using Trizol (Invitrogen, Thermo Scientific, USA). The purity and integrity of RNA were checked using agarose gel electrophoresis and a Qubit 4 fluorometer (Invitrogen, USA). Maxima cDNA Kit (ThermoScientific, USA) was utilized to make the cDNA, following the manufacturer's instructions.

Simply mix 0.5 µg of total RNA with 1 µL of dsDNase, 1 µL of 10X dsDNase buffer, and 10 µL water, then gently mix and centrifuge. To allow the reaction mixture to incubate, the thermomixer was preheated to 37 °C for 2 min. 20 µL were obtained by mixing 4 µL of Reaction Mix, 2 µL of Maxima Enzyme Mix, and 4 µL of nuclease-free water. Finally, qRT-PCR was implemented to detect gene expressions of anti-inflammatory genes like NF-κβ, COX2, IL-6, and TNF-α, apoptotic genes such as PI3K, Akt, Caspase3, and mTOR, and proinflammatory genes such as cyclinD1 and Bcl2. We performed 40 cycles of 55 °C for 15 sec, followed by 40 cycles of 55 °C for 60 sec. The 2-ΔΔCt approach was utilized to detect

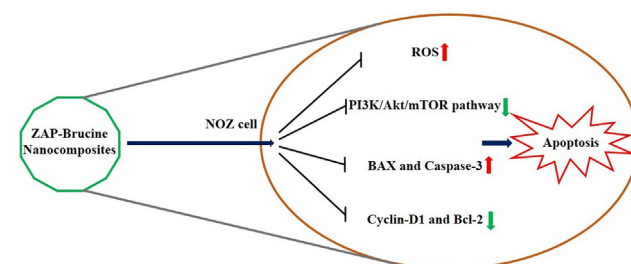


Fig 1 Proposed mechanisms of ZAP-Bru nanocomposites on NOZ cells.

the expression levels, and they were expressed as fold changes compared to untreated control.

2.11. Statistical analysis

SPSS 20.0 was utilized to analyze the obtained data (SPSS Inc., Chicago, Illinois, USA). All data are represented as mean \pm SD. We used one-way ANOVA as the statistical comparison method and Tukey's test for further confirmation. Statistical significance was determined at $P < 0.05$.

3. Results

3.1. Characterization of ZAP-Bru NCs

ZAP-Bru NCs containing ZAP-Bru exhibit UV-vis absorption spectra between 400 and 1000 nm as shown in Fig. 2A. The absorption bands in the spectra of the NCs containing ZAP-Bru NCs show that nanostructured ZAP-Bru NC materials exhibit an intense absorption maximum centered at around 360 nm. FT-IR analysis was utilized to detect the various functional groups in ZAP-Bru NCs (2B). The peaks represent functional groups in the ZAP-Bru NCs. As a result, the absorption peaks in the samples are identified as 3443 cm^{-1} , 2855 cm^{-1} , 1650 cm^{-1} , 1109 cm^{-1} , 951 cm^{-1} , 852 cm^{-1} , and 614 cm^{-1} . Metal-oxygen stretching vibrations are linked to the absorption peak at 614 cm^{-1} (ZAP-Bru NCs). A vibration of the main alcohol's C-N or C-O bonds is what causes the peak at

1109 cm^{-1} . The peak at 1650 cm^{-1} is due to the molecular vibration modes of aromatic nitro compounds and alkyls. Peaks at 2855 cm^{-1} and 3443 cm^{-1} are caused by stretching vibrations of hydroxyl compounds. Fig. 2B depicts the FTIR spectra of ZAP-Bru NCs. Using FTIR analysis, it is feasible to watch the vibrations of specific atoms or collections of atoms. The results showed a high prevalence of ZAP-Bru NC bonds. The result of combining ZAP-Bru NCs is shown in Fig. 2C, which exhibits a unique band at about 478 nm that is centered on the graph of the PL spectra.

Fig. 3A and 3B depict the structural characterization of ZAP-Bru NCs. The structures were homogeneous and evenly distributed; however, at the magnification employed, they appeared more insulated and crowded. We obtain a higher particle size by including particle dispersion in our EDAX calculation. Fig. 3C displays the EDAX result for ZAP-Bru NCs. The weight percentages of carbon, nitrogen, and oxygen should be 7.10%, 52.60%, 2.06%, and 38.25%, respectively, according to stoichiometric calculations. ZAP-Bru NCs are chemically similar to these percentages, as shown by the Zn, C, N, and O.

ZAP-Bru NCs of a hexagonal ZAP-Brucine phase (wurtzite structure) were analyzed via X-ray diffraction. Several parameters related to the lattice structure are given, including hexagonal unit cells. Based on the literature values (Maguire et al., 1982), ZAP-Brucine peaks and relative intensities matched those obtained in the literature for the other components. Impurity peaks did not exhibit characteristic characteristics. The peaks are at scattering angles of 31.64° , 34.85° , 36.65° ,

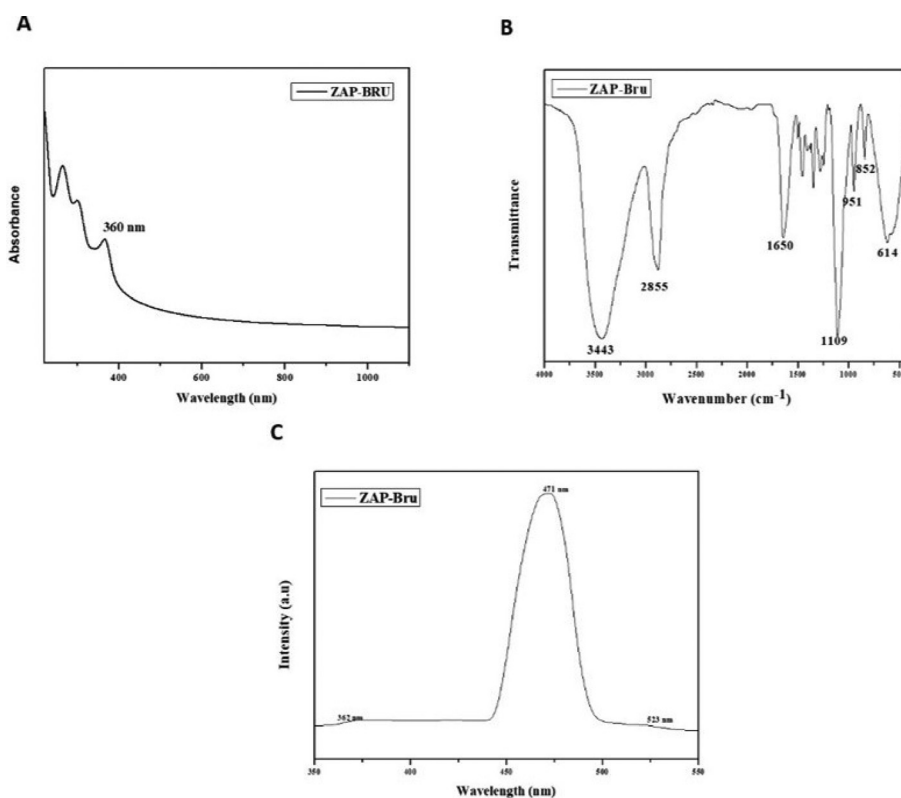


Fig. 2 Characterization analysis of ZAP-Bru nanocomposites. (a). UV-vis absorption spectra (400–1000 nm). (b). FTIR Transmittance vs wavenumber chart of ZAP-Bru nanocomposites derived from infrared analysis. (c). Photoluminescence spectra for ZAP-Bru nanocomposites at room temperature.

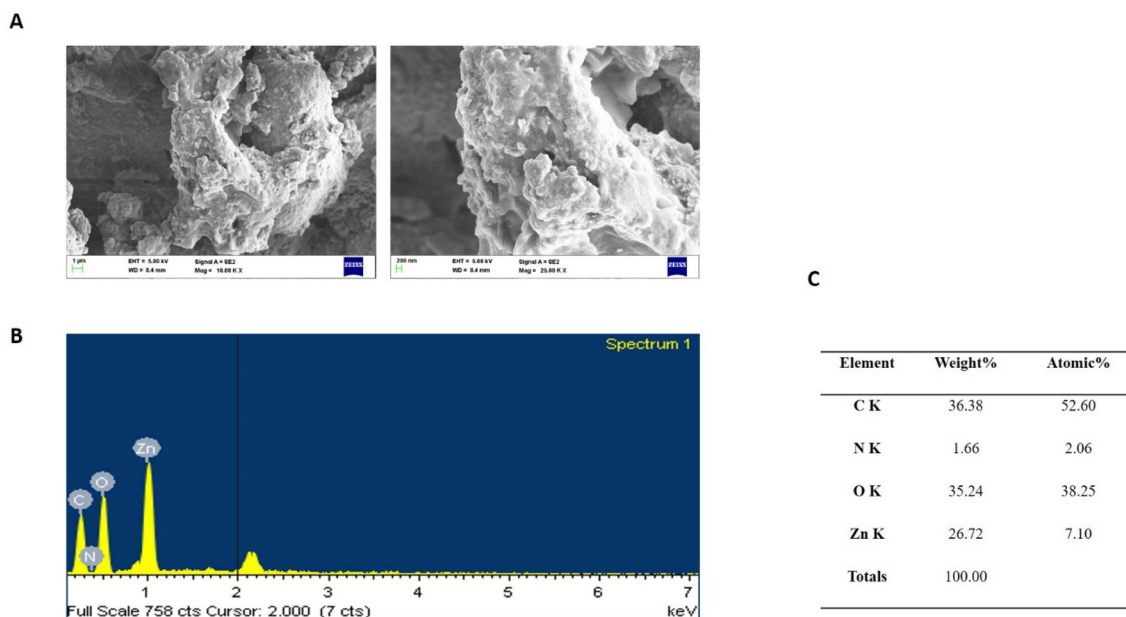


Fig. 3 SEM micrographics of the ZAP-Bru nanocomposites. Up and down surface area (a), parts and the respective compositions obtained by EDX elements, weight % and atomic % of the composition obtained by EDX (b & c).

46.1°, 57.12°, 63.2°, and 68.9°, which correspond to 100, 002, 101, 102, 110, 103, and 112 in the crystal plane, respectively. ZAP-Bru NCs with the XRD demonstrated above have an average size of 19.23 nm based on the Scherrer formula (Fig. 4A). The ZAP-Bru NCs (numerically weighted) are shown in Fig. 4B. At room temperature, we obtained the smallest particles. In comparison with other analytical techniques, this method showed smaller particle sizes, indicating a high degree of clustering. Electrostatics and Van der Waals forces are responsible for the interactions between particles.

3.2. The cytotoxicity of ZAP-Bru NCs in NOZ cells

Fig. 5 shows the results of a 24-hour cytotoxicity study of NOZ cells treated with ZAP-Bru NCs at six several dosages (1, 2.5, 5, 7.5, 10, & 15 µg/ml). A reduction in cell viability is noted in the NOZ cells after treatment with increased dosages of ZAP-Bru NCs. Treatment with 5 µg/ml resulted in the decrease of viable cells with 50%, hence it was fixed as IC50

concentration. Therefore, 5 and 7.5 µg/ml of ZAP-Bru NCs were selected for further study as an IC50 and high dose, respectively, because a concentration of 5 µg/ml of ZAP-Bru NCs produced 50% of cell death (Fig. 5).

3.3. The ZAP-Bru NCs induced apoptosis in NOZ cells

ZAP-Bru NCs treatment-induced apoptosis in the NOZ cells were examined by dual staining, and the outcomes were revealed in Fig. 6. A higher green fluorescence is noted in the control cells, whereas higher yellow and orange fluorescence was noted in 5 and 7.5 µg/ml of ZAP-Bru NCs-treated NOZ cells, which reveals the increased apoptotic incidences (Fig. 6).

3.4. The ZAP-Bru NCs induced ROS accumulation in NOZ cells

A DCFH-DA staining was performed on NOZ cells to detect the ZAP-Bru NCs treatment-induced intracellular ROS accu-

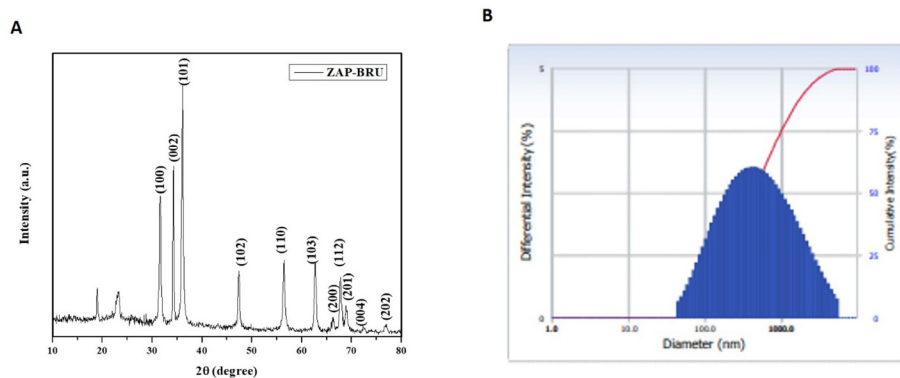


Fig. 4 XRD Pattern and DLS analysis of ZAP-Bru nanocomposites. (a). XRD analysis (b). Number-weighted particle size distribution, obtained by DLS.

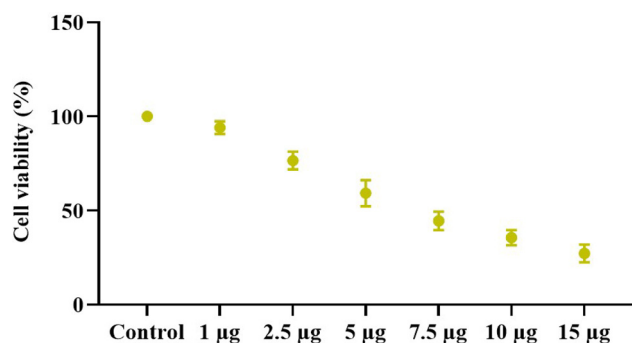


Fig. 5 ZAP-Bru nanocomposites cause cytotoxicity in NOZ cells. NOZ cell lines from human GBC cell lines were treated with ZAP-Bru nanocomposites (1–15 µg) for 24 h. The cells were subjected to MTT assay and the values were depicted as \pm SD of three individual experiments.

mulation. Control cells demonstrated only mild or dull green fluorescence, whereas 5 and 7.5 µg/ml of ZAP-Bru NCs treated NOZ cells exhibited higher green fluorescence than control. These outcomes suggest a higher accumulation of ROS in the ZAP-Bru NCs-treated NOZ cells (Fig. 6).

3.5. MMP level in NOZ cells is impaired by ZAP-Bru NCs

The status of MMP in the control and ZAP-Bru NCs treated NOZ cells was assessed by the Rh-123 staining, and the outcomes are revealed in Fig. 6. The untreated control cells demonstrated a higher green fluorescence, whereas the treatment with 5 and 7.5 µg/ml of ZAP-Bru NCs demonstrated a

dull or reduced green fluorescence in the NOZ cells. These findings obviously suggest that the ZAP-Bru NCs appreciably decreased the MMP status in the NOZ cells (Fig. 6).

3.6. Effect of ZAP-Bru NCs on cell adhesion of NOZ cells

The cell adhesion assay was performed on the NOZ cells treated with synthesized ZAP-Bru NCs. Compared to cells treated with ZAP-Bru NCs, the untreated control group showed an increase in viable cells. The 5 µg of ZAP-Bru NCs treatment decreased the number of viable cells. The 7.5 µg of ZAP-Bru NCs treatment also drastically increased the dead cells when compared with control (Fig. 7).

3.7. An assessment of gene expression levels associated with inflammation

As revealed in Fig. 8, the alterations in gene expression of NF- κ B, IL-6, COX-2, and TNF- α are seen in NOZ cells after ZAP-Bru NCs treatment for 24 h. To calculate the fold changes in gene expression levels with each gene, we compared them to untreated NOZ cells. In this study, we observed a decrease in pro-inflammatory gene expression after treating NOZ cells for 24 h with 5 and 7.5 µg of ZAP-Bru NCs.

3.8. ZAP-Bru NCs treatment induces apoptosis in the NOZ cells

As shown in Fig. 9, ZAP-Bru NCs induced apoptosis in NOZ cells by down-regulating anti-apoptotic genes such as PI3K, AKT, mTOR, and CyclinD1 and up-regulating pro-apoptotic genes Bcl2 and caspase-3. 5 and 7.5 µg of ZAP-Bru NCs decreased PI3K, AKT, mTOR, and CyclinD1 expres-

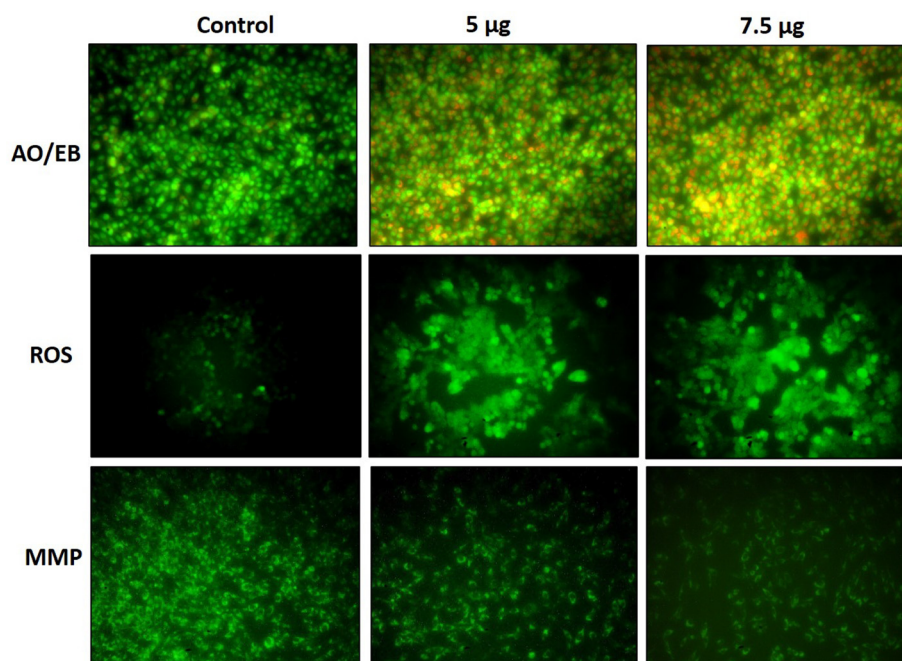


Fig. 6 NOZ cells are apoptotic when treated with ZAP-Bru nanocomposites. NOZ cell lines of human GBC cell lines were treated with ZAP-Bru nanocomposites for 24 h. Acridine orange and ethidium bromide (1:1), was used to stain the cells. The NOZ cell line is subjected to oxidative stress induced by ZAP-Bru nanocomposites were staining with DCFH-DA. NOZ cells with ZAP-Bru nanocomposites present have a decreased mitochondrial membrane permeability. Rhodamine 123 was used to stain the cells.

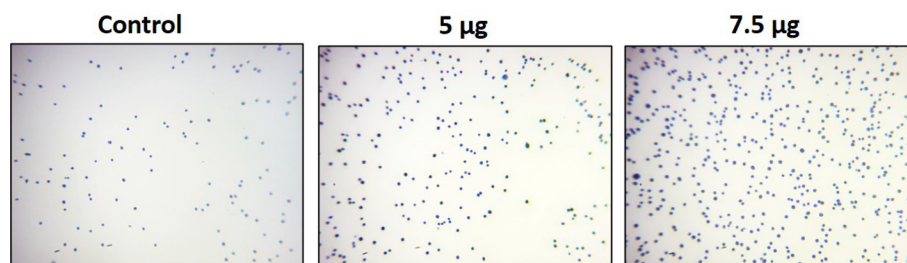


Fig. 7 Cell adhesion is impaired by ZAP-Bru nanocomposites in NOZ cells. ZAP-Bru nanocomposites and doxorubicin were used to treat human GBC cell line NOZ cell lines. In the following figures, representative stained cells of the control and treated groups were shown in cell adhesion assays. Control, ZAP-Bru nanocomposites-treated cells; 5 μg concentration and 7.5 μg concentration.

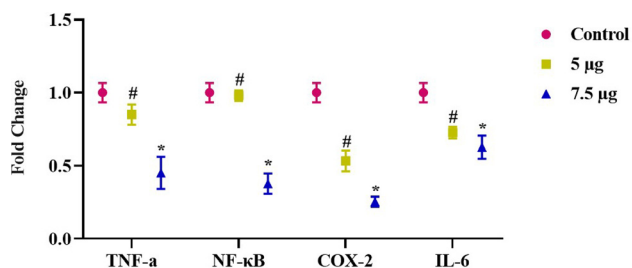


Fig. 8 Gene expression changes induced inflammatory response in NOZ cell line. Expression of NF- κB , IL-6, Cox-2, and TNF- α in mRNA level after 24-h treatment of 5 & 7.5 μg concentration of ZAP-Bru nanocomposites. The data were presented as folds change compared to the untreated “Control” cells and mean \pm SEM. $n = 6$, * $p < 0.005$ compared to the “Control” group, # $p < 0.05$ compared to “control” group.

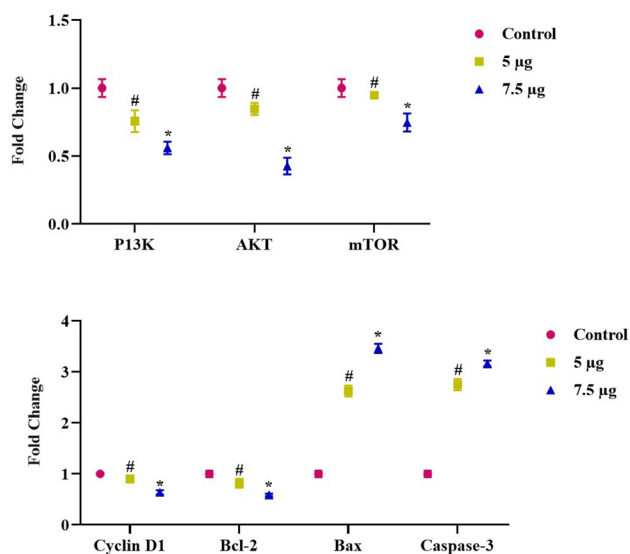


Fig. 9 Gene expression changes induced apoptotic cell death in NOZ cell line. Expression of anti-apoptotic genes such as PI3K, AKT, mTOR, and CyclinD1 and upregulating pro-apoptotic gene Bcl2 and caspase-3 in mRNA level after 24-h treatment of 5 & 7.5 μg concentration of ZAP-Bru nanocomposites. The data were presented as folds change compared to the untreated “Control” cells and mean \pm SEM. $n = 6$, * $p < 0.005$ compared to the “Control” group, # $p < 0.05$ compared to “control” group.

as well as Bcl2 in a dose-dependently. NOZ cells, however, appear to undergo apoptosis via the caspase-dependent mitochondrial-mediated intrinsic pathway, as indicated by increases in Bax and caspase-3 expression.

4. Discussion

Malignant tumors with distinctive biological characteristics, like the human GBC, are incredibly aggressive and challenging to detect. Surgery to remove the tumor, chemotherapy, and radiotherapy are all ineffective treatments for the GBC. Based on detailed research of biological features and metastatic pathways, it is important to design novel adjuvant medications, potential antitumor agents, and GBC that can be treated utilizing molecularly targeted approaches. With the majority of biological molecules existing, forming, and performing their roles at the nanoscale, nanomedicine aims to address these issues.

The ZAP-Bru NCs absorption peak was found at 360 nm, showing that there is an inherent bandgap in UV-Vis spectra (Fig. 1a). Similar results were observed in earlier research for the ZAP-Bru NCs absorption region, which has a wavelength range of 355–380 nm (Zak et al., 2011; Bian et al., 2011; Lavand et al., 2018). Utilizing FT-IR, the functional groups of the synthesized ZAP-Bru NCs were examined and identified (Fig. 1b). A wide absorption band with ZAP-Bru NCs stretching vibration was discovered at 614 cm^{-1} during FT-IR spectrum analysis. There was also evidence of FT-IR having a band at 400 cm^{-1} in earlier studies with ZAP-Bru NCs (Zak et al., 2011). The ZAP-Bru NCs SEM study showed that they were evenly dispersed, closely related in size, and grouped by shape (Fig. 2a and 2b). Controlling the stoichiometry and purity of ZAP-Bru NCs was made possible with the help of EDS analysis. There are no impurity peaks evident in the EDS pattern, which confirms the presence of Zn, C, N, and O elements (Fig. 2c). The distribution of each element was determined using the relevant K line from the X-ray spectra (C, O, N, and Zn). The samples are largely homogeneous, according to the EDS mapping pictures, with some localized NCs aggregation forming as the ZAP-Bru NCs proportion increases (Motelica et al., 2021). The residual peaks are indexed to the hexagonal structure of ZAP-Bru NCs, which is in agreement with the standard data no. 36–1451 (Gawande and colleagues, 2015). The XRD outcomes revealed that the precursors had entirely changed into ZAP-Bru NCs crystals after calcination. The strong and crisp peaks indicate the presence of well-ordered crystalline materials (Fig. 3a).

Our cytotoxicity findings are consistent with other research that found ZAP- Brucine NPs dramatically promote cytotoxicity.

city in cancer cells (Fig. 4) while having no significant effect on normal cells. Some human glioma cell lines (LNZ308, LN18, A172, LN229, and U87) were found to be cytotoxic by ZAP-Brucine NPs, but normal human astrocytes were found to be unaffected (Ostrovsky et al., 2009). It was already demonstrated that Zn-based NPs preferentially (or exclusively) cause cancer cells to undergo apoptosis than normal cells (Hanley et al., 2008). Higher ROS and the cytotoxicity of nano-sized substances have already been supported by earlier literature (Nel et al., 2006). As an activator of cell growth and development in both normal and stressed conditions, ROS can perform a number of functions. However, under stressful situations, it can also result in CD in addition to pathological defects (cell death). High levels of intracellular ROS cause the apoptotic process to begin (Hu et al., 2009). It is crucial to screen the mitochondrion's depolarized membrane because of the dysfunction of responsive genes.

BCL-2 and caspases are triggered when the mitochondrial membrane is damaged, preventing the synthesis of genes that are receptive to cancer cells. Rhodamine 123 was delivered into the mitochondrial membrane, which caused intracellular leakage materials to disappear. The color of these materials shifted from red to green, suggesting the onset of apoptosis (Momtazi-Borojeni et al., 2013). Our results showed that the NF- κ B, IL-6, COX-2, and TNF- α genes were downregulated when treated with 5 and 7.5 μ g/ml of ZAP-Bru NCs when compared to control NOZ cells (Fig. 7). RIP-1, a receptor-interacting protein that promotes NF- κ B (p65) activation, is upregulated in the GBC. TNF-stimulated IKK/NF- κ B activation is complicated by the ubiquitination of RIP1. During GBC pathogenesis, several genes encoding transcription factors and cell signaling regulators had their expression altered as well, implying that their interactions with their corresponding p53 proteins are disrupted (Zhu et al., 2014; Xu et al., 2010). Chemokines, MMP-9, TNF- α , IL-1 β , IL-6, 5-LOX, COX-2, and VEGF are among the hundreds of pro-inflammatory regulators activated by NF- κ B upregulation (Aggarwal et al., 2006). mRNA expression levels of ZAP-Bru NCs induced apoptosis in NOZ cells by down-regulating anti-apoptotic and upregulating pro-apoptotic genes (Fig. 8). Jin et al. (2015) suggested that the curcumin up-regulating miR-192-5p expression and down-regulates the PI3K/Akt signaling pathway, thereby causing apoptosis in human lung cancer cells, which supports our findings.

5. Conclusion

In conclusion, the present findings prove that ZAP-Bru NCs have anti-cancer effects on the human GBC NOZ cell line. Our results demonstrate that ZAP-Bru NCs treatment effectively inhibited the growth, induced apoptosis, and inhibited the PI3K/Akt/mTOR pathway in the NOZ cells. Therefore, it was clear that ZAP-Bru NCs could be utilized as a novel anticancer agent in the future.

Funding

Nil.

Conflict of interest

The authors declare no conflict of interest

References

- Abdollahi, A., Goldanlou, A.S., Golmohammadeh, A., 2021. Effects of surfactant on thermal conductivity of aqueous silica nanofluids. *J Mol Liquid.* 327, (1) 114883.
- Aggarwal, B.B., Shishodia, S., Sandur, S.K., Pandey, M.K., Sethi, G., 2006. Inflammation and cancer: how hot is the link? *Biochem Pharmacol.* 72 (11), 1605–1621.
- Bian, S.W., Mudunkotuwa, I.A., Rupasinghe, T., Grassian, V.H., 2011. Aggregation and dissolution of 4 nm ZAP- Brucine nanocomposites in aqueous environments: influence of pH, ionic strength, size, and adsorption of humic acid. *Langmuir* 27 (10), 6059–6068.
- Bray, F., Ferlay, J., Soerjomataram, I., Siegel, R.L., Torre, L.A., Jemal, A., 2018. Global cancer statistics 2018: GLOBOCAN estimates of incidence and mortality worldwide for 36 cancers in 185 countries. *CA Cancer J Clin.* 68 (6), 394–424.
- Caputo, F., de Nicola, M., Ghibelli, L., 2014. Pharmacological potential of bioactive engineered nanomaterials. *BiochemPharmacol.* 92, 112–130.
- Fernandes, E., Ferreira, J.A., Peixoto, A., et al, 2015. New trends in guided nanotherapies for digestive cancers: a systemic review. *J Control Release.* 209, 288–307.
- Fru, P.N., Nweke, E.E., Mthimkhulu, N., Mvango, S., Nel, M., Pilcher, L.A., Balogun, M., 2021. Anti-Cancer and Immunomodulatory Activity of a Polyethylene Glycol-Betulinic Acid Conjugate on Pancreatic Cancer Cells. *Life.* 11 (6), 462.
- Goldin, R.D., Roa, J.C., 2009. Gallbladder cancer: a morphological and molecular update. *Histopathology* 55 (2), 218–229. <https://doi.org/10.1111/j.1365-2559.2008.03192.x>.
- Hanley, C., Layne, J., Punnoose, A., Reddy, K.M., Coombs, I., Coombs, A., Feris, K., Wingett, D., 2008. Preferential killing of cancer cells and activated human T cells using ZAP- Brucine nanocomposites. *Nanotech.* 19, (29) 295103.
- Hu, R., Yong, K.T., Roy, I., Ding, H., He, S., Prasad, P.N., 2009. Metallic nanostructures as localized plasmon resonance enhanced scattering probes for multiplex dark-field targeted imaging of cancer cells. *J Phys Chem. C.* 113, 2676–2684.
- Huang, M., Borzoei, H., Abdollahi, A.A., Li, Z., Karimipour, A., 2021. Effect of concentration and sedimentation on boiling heat transfer coefficient of GNPs-SiO₂/deionized water hybrid Nanofluid: An experimental investigation. *Int Communication Heat Mass Transfer.* 122, 105141.
- Jin, H., Qiao, F., Wang, Y., Xu, Y., Shang, Y., 2015. Curcumin inhibits cell proliferation and induces apoptosis of human non-small cell lung cancer cells through the upregulation of miR-192-5p and suppression of PI3K/Akt signaling pathway. *Oncol Rep.* 34 (5), 2782–2789.
- Lavand, A.B., Malghe, Y.S., 2018. Synthesis, characterization and visible light photocatalytic activity of carbon and iron modified ZAP-Brucine. *Journal of King Saud University-Science.* 30 (1), 65–74.
- Li, M., Li, P., Zhang, M., Ma, F., 2018. Brucine suppresses breast cancer metastasis via inhibiting epithelial-mesenchymal transition and matrix metalloproteinases expressions. *Chin. J. Integr. Med.* 24 (1), 40–46.
- Mody, V.V., Siwale, R., Singh, A., et al, 2010. Introduction to metallic nanocomposites. *J Pharm Bioallied Sci.* 2, 282–289.
- Momtazi-borojeni, A.A., Behbahani, M., Sadeghi-aliabadi, H., 2013. Antiproliferative activity and apoptosis induction of crude extract and fractions of *Avicennia Marina*. *Iran J Basic Med Sci.* 16, 1–10.
- Motelica, L., Fica, D., Oprea, O., Fica, A., Trusca, R.-D., Andronescu, E., Holban, A.M., 2021. Biodegradable Alginate Films with ZAP-Brucine Nanocomposites and Citronella Essential Oil—A Novel Antimicrobial Structure. *Pharmaceutics.* 13 (7), 1020.
- Nel, A., Xia, T., Mädler, L., Li, N., 2006. Toxic potential of materials at the nanolevel. *Science* 311 (5761), 622–627. <https://doi.org/10.1126/science>.

- Ostrovsky, S., Kazimirsky, G., Gedanken, A., Brodie, C., 2009. Selective cytotoxic effect of ZAP- Brucine nanocomposites on glioma cells. *Nano Res.* 2, 882–890.
- Peng, Y., Ghahnaviye, M.B., Ahmad, M.N., Addollahi, A.A., Bagherzadeh, S.A., Azimy, H., Mosavi, A., Karimpour, A., 2021. Analysis of the effect of roughness and concentration of Fe₃O₄/water nanofluid on the boiling heat transfer using the artificial neural network: An experimental and numerical study. *Int J Thermal Sci.* 163, 106863.
- Randi, G., Franceschi, S., La Vecchia, C., 2006. Gallbladder cancer worldwide: geographical distribution and risk factors. *Int J Cancer.* 118 (7), 1591–1602.
- Rasmussen, J.W., Martinez, E., Louka, P., et al, 2010. Zinc oxide nanocomposites for selective destruction of tumor cells and potential for drug delivery applications. *Exp Opin Drug Deliv.* 7, 1063–1077.
- Salimpour, M.R., Karimi Darvanjooghi, M.H., Abdollahi, A., Karimpour, A., Goodarzi, M., 2020. Providing a model for Csf according to pool boiling convection heat transfer of water/ferrous oxide nanofluid using sensitivity analysis. *Int. J. Numer. Meth. Heat Fluid Flow* 30 (6), 2867–2881.
- Shi, X., Zhu, M., Kang, Y., Yang, T., Chen, X., Zhang, Y., 2018. Wnt/ β -catenin signaling pathway is involved in regulating the migration by effective natural compound brucine in LoVo cells. *Phytomedicine.* 15 (46), 85–92.
- Sturm, N., Schuhbaur, J.S., Hüttner, F., Perkhofer, L., Ettrich, T. J., 2022. Gallbladder Cancer: Current Multimodality Treatment Concepts and Future Directions. *Cancers (Basel).* 14 (22), 5580.
- Tshweu, L.L., Shemis, M.A., Abdelghany, A., Gouda, A., Pilcher, L. A., Sibuyi, N.R.S., Meyer, M., Dube, A., Balogun, M.O., 2020. Synthesis, physicochemical characterization, toxicity and efficacy of a PEG conjugate and a hybrid PEG conjugate nanoparticle formulation of the antibiotic moxifloxacin. *RSC Adv.* 10, 19770–19780.
- Xu, G., Tan, X., Wang, H., Sun, W., Shi, Y., Burlingame, S., Gu, X., Cao, G., Zhang, T., Qin, J., Yang, J., 2010. Ubiquitin-specific peptidase 21 inhibits tumor necrosis factor alpha-induced nuclear factor kappaB activation via binding to and deubiquitinating receptor-interacting protein 1. *J Biol Chem.* 285 (2), 969–978.
- Zak, A.K., Razali, R., Abd Majid, W.H., Darroudi, M., 2011. Synthesis and characterization of narrow size distribution of zinc oxide nanocomposites. *Int. J. Nanomed.* 6, 1399.
- Zhang, H., Chen, B., Jiang, H., Wang, C., Wang, H., Wang, X., 2011. A strategy for ZAP- Brucine nanorod mediated multi-mode cancer treatment. *Biomaterials* 32, 1906–1914.
- Zhu, G., Chen, X., Wang, X., Li, X., Du, Q., Hong, H., Tang, N., She, F., Chen, Y., 2014. Expression of the RIP-1 gene and its role in growth and invasion of human gallbladder carcinoma. *Cell Physiol Biochem.* 34 (4), 1152–1165.
- Zhu, Z., Luo, K., Zhang, B., Wang, G., Guo, K., Huang, P., Liu, Q., 2023. Risk factor analysis and construction of prediction models of gallbladder carcinoma in patients with gallstones. *Front Oncol.* 13, 1037194.